Developmental Biology 344 (2010) 52–65

Contents lists available at ScienceDirect

Developmental Biology

journal homepage: www.elsevier.com/developmentalbiology

Tuning sperm chemotaxis by calcium burst timing

Adan Guerrero [a], Takuya Nishigaki [a], Jorge Carneiro [b], Yoshiro Tatsu [c], Christopher D. Wood [a,*], Alberto Darszon [a]

[a] Departamento de Genética del Desarrollo y Fisiología Molecular, Instituto de Biotecnología, Universidad Nacional Autónoma de México, Cuernavaca, Morelos, México
[b] Instituto Gulbenkian de Ciência, Oeiras, Portugal
[c] National Institute of Advanced Industrial Science and Technology (AIST), Midorigaoka, Ikeda, Japan

ARTICLE INFO

Article history:
Received for publication 14 December 2009
Revised 8 April 2010
Accepted 12 April 2010
Available online 16 May 2010

Keywords:
Chemotaxis
Fertilization
Flagella
Sperm motility
Ca^{2+} signaling
Sea urchin sperm

ABSTRACT

Marine invertebrate oocytes establish chemoattractant gradients that guide spermatozoa towards their source. In sea urchin spermatozoa, this relocation requires coordinated motility changes initiated by Ca^{2+}-driven alterations in sperm flagellar curvature. We discovered that *Lytechinus pictus* spermatozoa undergo chemotaxis in response to speract, an egg-derived decapeptide previously noted to stimulate non-chemotactic motility alterations in *Strongylocentrotus purpuratus* spermatozoa. Sperm of both species responded to speract gradients with a sequence of turning episodes that correlate with transient flagellar Ca^{2+} increases, yet only *L. pictus* spermatozoa accumulated at the gradient source. Detailed analysis of sperm behavior revealed that *L. pictus* spermatozoa selectively undergo Ca^{2+} fluctuations while swimming along negative speract gradients while *S. purpuratus* sperm generate Ca^{2+} fluctuations in a spatially non-selective manner. This difference is attributed to the selective suppression of Ca^{2+} fluctuations of *L. pictus* spermatozoa as they swim towards the source of the chemoattractant gradient. This is the first study to compare and characterize the motility components that differ in chemotactic and non-chemotactic spermatozoa. Tuning of Ca^{2+} fluctuations and associated turning episodes to the chemoattractant gradient polarity is a central feature of sea urchin sperm chemotaxis and may be a feature of sperm chemotaxis in general.

Introduction

Union of the male and female gametes is a necessary condition for the propagation of sexually reproductive species. In many species, including mammals, spermatozoa are guided in their journey towards the egg or oocyte by gradients of chemical signals released by the female gamete or its associated structures, a mechanism known as chemotaxis (reviewed in Eisenbach and Giojalas, 2006). By effectively increasing the size of the egg or oocyte from tens or hundreds of micrometers to up to millimeters or more, the probabilities of spermatozoa–egg union are enhanced (Podolsky, 2001; 2002).

Spermatozoa chemotaxis has been most widely documented in marine invertebrates that undergo external fertilization (Miller, 1985b). Most commonly the spermatozoa redirect their swimming paths towards the source of a chemoattractant gradient through stereotypical sequences of turns interspersed by periods of straighter swimming (hereafter referred to as the "turn-and-run" pattern) (Bohmer et al., 2005; Kaupp et al., 2003). This redirection is driven by increases in flagellar curvature during turns, and decreases in curvature during the episodes of straighter swimming (Kaupp et al., 2003). This phenomenon has been observed in diverse marine phyla, although until now the only reported sea urchin to display chemotactic spermatozoa motility is *Arbacia punctulata* (Bohmer et al., 2005; Kaupp et al., 2003; Miller, 1985a; Ward et al., 1985).

Sea urchin spermatozoa motility is modulated by spermatozoa-activating peptides (SAP), a diverse group of peptides that have been isolated from the egg investments of a variety of sea urchin species (Suzuki, 1995). The first characterized and most widely studied member of the SAP family is speract (GFDLNGGGVG), from *Strongylocentrotus purpuratus* sea urchin eggs (Hansbrough and Garbers, 1981; Suzuki et al., 1981). Current models propose that after speract binds to its receptor in the flagellum, activation of guanylate cyclase activity increases cyclic GMP (cGMP) levels, which hyperpolarizes the spermatozoa through opening of cGMP-regulated K^+ channels (Bonigk et al., 2009; Darszon et al., 2001, 2005; Galindo et al., 2007; Strunker et al., 2006). It is speculated that hyperpolarization removes inactivation from voltage-gated Ca^{2+} channels, which subsequently open following a depolarization (Granados-Gonzalez et al., 2005; Strunker et al., 2006). This fast transient increase in flagellar $[Ca^{2+}]_i$ has been associated with the transient increases in flagellar bending that prompt sea urchin spermatozoa to undergo a turning event (Babcock et al., 1992; Bohmer et al., 2005; Kaupp et al., 2003; Wood et al., 2003) (reviewed in Darszon et al., 2008). Extracellular Ca^{2+} is required for all recorded instances of gamete

* Corresponding author. Instituto de Biotecnología, UNAM, Avenida Universidad 2001, Col. Chamilpa, Cuernavaca, Morelos, Mexico. Fax: +52 777 3172388.
E-mail address: chris@ibt.unam.mx (C.D. Wood).

0012-1606/$ – see front matter © 2010 Elsevier Inc. All rights reserved.
doi:10.1016/j.ydbio.2010.04.013

chemotaxis and inhibition of Ca^{2+}-permeable cation channels in ascidian spermatozoa blocks chemotaxis (Miller, 1985a; Yoshida et al., 2002). The absence of external Ca^{2+} abolishes the phasic Ca^{2+} increases, the turning events, and as shown in the sea urchin *A. punctulata*, chemotaxis (Kaupp et al., 2003).

Speract-stimulated *S. purpuratus* spermatozoa redirect their swimming paths with a stereotypical turn-and-run pattern, but under laboratory conditions do not show chemotaxis towards speract or egg investments (reviewed in Darszon et al., 2008). In *Lytechinus pictus* sperm, speract is also reported to increase intracellular Ca^{2+}, cyclic nucleotide concentration and mitochondrial respiration (Bentley and Garbers, 1986; Bentley et al., 1986; Nishigaki and Darszon, 2000), however motility responses have not been reported. At least two speract isoforms have been isolated from *L. pictus* egg-associated structures: GFDLTGGGVQ ([Thr^5, Gln^{10}] speract) and FDLTGGGVQ ([Des-Gly^1, Thr^5, Gln^{10}] speract), which conserve the functionally important glycine residue at position 6 found in all other reported members of the speract-related SAPs isolated from eggs of seven species of the Echinoida order (Suzuki, 1995). Here we characterize the motility response of *L. pictus* spermatozoa to uncaged ([Ser^5, NB-Gly^6] speract) (Tatsu et al., 2002), which compared to canonical speract has a largely indistinguishable binding affinity and induced metabolic response in *S. purpuratus* sperm (Tatsu et al., 2002), and which hereon in is referred to as simply speract. We report that *L. pictus* spermatozoa accumulate at the source of a speract gradient via chemotactic redirection of their swimming paths. Interestingly, under the same experimental condition *S. purpuratus* spermatozoa showed re-localization but not chemotaxis. Thus the spermatozoa of two phylogenetically closely-related sea urchins react to speract gradients with turn-and-run type motility responses, yet the result is chemotaxis in only one of those species.

Our findings suggest that the ability of *L. pictus* spermatozoa to selectively increase flagellar Ca^{2+} and curvature while experiencing a negative chemoattractant gradient (and/or suppress flagellar Ca^{2+} and curvature while experiencing a positive chemoattractant gradient) is an essential component that characterizes chemotactic motility in sea urchin spermatozoa, and possibly chemotactic spermatozoa motility in general. Furthermore, we discovered that this biased response was confined to a short temporal window within the first 3–5 s after speract exposure. This initial chemotactic phase was followed by an apparently adapted response to the source of the concentration gradient that might promote spermatozoa–egg union once spermatozoa arrive in the immediate vicinity of the egg. This is the first study to compare and characterize the motility components that differ in chemotactic and non-chemotactic spermatozoa.

Materials and methods

Materials

Spermatozoa were obtained undiluted from *S. purpuratus* or *L. pictus* (Marinus Inc., Long Beach, CA, USA; Pamanes S. A. de C.V., Ensenada, Mexico) by intracoelomic injection of 0.5 M KCl and stored on ice until used within a day. Artificial seawater (ASW) was 950–1000 mOsm and contained (mM): 486 NaCl, 10 KCl, 10 $CaCl_2$, 26 $MgCl_2$, 30 $MgSO_4$, 2.5 $NaHCO_3$, 10 HEPES and 1 EDTA (pH 8.0) for *S. purpuratus*. For experiments with *L. pictus* spermatozoa, slightly acidified ASW (pH 7.4) was used to reduce the number of spontaneous acrosomally reacted spermatozoa. Low Ca^{2+} ASW was as ASW but pH 7.0 and with 1 mM $CaCl_2$, and Ca^{2+}-free ASW was ASW with no added $CaCl_2$. [Ser^5; nitrobenzyl-Gly^6]speract, referred to throughout the text as 'caged speract', was prepared as previously described (Tatsu et al., 2002). Fluo-4-AM and pluronic F-127 were from Molecular Probes, Inc. (Eugene, OR, USA). PolyHEME (poly(2-hydroxyethyl methacrylate)) and other reagents, unless indicated, were from Sigma-Aldrich (Toluca, Edo de Mexico, Mexico).

Loading of Ca^{2+} fluorescent indicator into spermatozoa

Undiluted spermatozoa were suspended in 10 volumes of low Ca^{2+} ASW containing 0.2% wt/vol pluronic F-127 and 20 μM of Fluo-4 AM and incubated for 2 h at 14 °C. Spermatozoa were stored in the dark and on ice until use. For *S. purpuratus* spermatozoa, after initial loading of the Ca^{2+} indicator, cells were diluted with 100 volumes of low Ca^{2+} ASW, centrifuged for 10 min at 1000 *g* and 4 °C, and resuspended in the original volume of low Ca^{2+} ASW.

Fluorescence imaging of swimming spermatozoa

All coverslips were briefly immersed into a 0.05–0.1% (wt/vol) solution of polyHEME in ethanol, hot-air blow-dried to rapidly evaporate the solvent, and mounted on reusable chambers fitting a TC-202 Bipolar temperature controller (Medical Systems Corp.). The temperature plate was mounted on a microscope stage (Eclipse TE 300; Nikon) and maintained at a constant 15 °C. Aliquots of labeled sperm were diluted in ASW and transferred to an imaging chamber (final concentration $\sim 2\times10^5$ cells ml^{-1}). Epifluorescence images were collected with a Nikon Plan Fluor 40× 1.3 NA objective using a Chroma filter set (ex, HQ470/40×; DC, 505DCXRU; em, HQ510LP) and recorded on a EMCCD Andor camera (DV887, Andor iXon). Fluorescence illumination was supplied by a Luxeon V Star Lambertian Cyan LED part # LXHL-LE5C (Lumileds Lighting LLC, San Jose, USA) attached to a custom-built stroboscopic control box. The LED was mounted into a FlashCube40 assembly with dichroic mirror M40-DC400 (Rapp Opto Electronic, Hamburg). LED output was synchronized to the Exposure Out signal of the EMCCD camera via the control box to produce a single 2 ms flash per individual exposure. The camera exposure time was set equivalent to flash duration (2 ms). Images were collected with Andor iQ 1.8 software (Andor Bioimaging, NC) at 120 fps in full-chip mode, binning = 4×4 (corresponding to 128×128 pixels that generate an observation field of 200×200 μm; each pixel after binning has dimensions of 1.56×1.56 μm). Photolysis of caged speract was via a fiber optic coupled Xenon UV lamp (UVICO, Rapp Opto Electronic) filtered through a UV band-pass filter (270–400 nm) connected to the FlashCube40 and triggered by TTL unit (Andor Bioimaging, NC) connected to a Master 8 pulse generator (A.M.P.I., Jerusalem, Israel). The internal diameter of the optical fiber was 4 mm.

Image processing

Sperm head trajectories and their curvatures were measured using BohBoh software v3.29 with the 'Tracking of Swimming Cells' module (BohBohSoft, Tokyo, Japan) (Baba and Mogami, 1985). Path curvature was calculated each four immediately sequential points and filtered using a local smoothing technique with bi-square weighting and polynomial regression (sampling proportion = 0.08, polynomial degree = 10, final interval between consecutive smoothed points = 33 ms) with Sigma Plot software v9 (Systat Software, Inc.). In preparing image stacks for analysis and movies, the background fluorescence (F0) was removed by generating an average pixel intensity time-projection image from the first 360 frames before uncaging which was then subtracted from each frame of the image stack by using the 'Image calculator' tool of ImageJ v1.4 (National Institutes of Health, USA). For Fig. 2, maximum pixel intensity time projections were created each 3 s from background-subtracted images before and after the UV flash. The change in $[Ca^{2+}]_i$ in the overall flagellum was measured with software created by Jorge Carneiro (source code available from the authors upon request, manuscript in preparation). Briefly, the algorithm integrates the

intensity of the pixels inside the flagellum (without the head pixels) in each frame after background subtraction, stated as F (Fig. 3). Due to the inability to measure basal $[Ca^{2+}]_i$ in flagella, these values are an underestimation of the true relative increase of $[Ca^{2+}]_i$ occurring in the flagella.

Sperm chemotaxis

Chemotactic behavior was quantified by the linear equation chemotaxis index (LECI) using different sampling windows sizes (3 , 6 and 9 s) before (control) and after caged speract photolysis. LECI is a parameter derived from the negative value of the coefficient $(-A)$ in the linear equation $(D = At + D_0)$ of the distance (D) to the source of chemoattractant gradient vs. time (t), with D_0 being the initial sperm position; positive LECIs indicate movement towards the chemoattractant source (Yoshida et al., 2002) (Fig. 5). The source of the '*xy*' speract gradient coordinates was estimated by identifying the centroid of the UV flash intensity '*xy*' distribution (Fig. 1).

Analysis of the sperm direction with respect to the speract gradient at the initiation of each Ca^{2+} fluctuation

For each sperm motility response to speract we determined both the position and direction vectors with respect to the gradient source, at the beginning of each Ca^{2+} fluctuation (black and red arrow in Fig. 7, respectively) and calculated their inner product to get the value of the α angle (see Fig. 7). Values of α from 0 to 90° correspond to Type $(-)$ Ca^{2+} fluctuations that occurred when the spermatozoon was swimming down the chemotactic gradient (away from the source). Values of α from 90 to 180° correspond to Type $(+)$ Ca^{2+} fluctuations that occurred when spermatozoa were swimming up the chemotactic gradient (towards the source). For α calculations, head trajectories were filtered with a Low Pass Filter transform 'LOWPASS.XFM' (sampling interval = 0.01 s, half power point of filter = 4 Hz; Sigma Plot software v9 (Systat Software, Inc.)) to reduce high frequency noise due to flagellar beat development. The initial positions immediately before stimulation (regarding $(+)$ and $(-)$ positioning in the gradient) were unbiased for all sperm subsets analyzed. For determining the UVpos and UVneg populations of sperm, the spermatozoa position relative to the gradient source was defined by calculating the angle ϕ. Values of ϕ between 0 and 180° identify spermatozoa that are swimming in a positive gradient, and ϕ values between 180 and 360° identify spermatozoa that are swimming in a negative gradient (Fig. 7A):

$$\phi(\alpha) = \begin{cases} \alpha + 90, & \alpha \leq 90^\circ \text{ and } I.P. = max \\ \alpha + 90, & \alpha \geq 90^\circ \text{ and } I.P. = max \\ 90 - \alpha, & \alpha \leq 90^\circ \text{ and } I.P. = min \\ 450 - \alpha, & \alpha \geq 90^\circ \text{ and } I.P. = min \end{cases}.$$

I.P. is the inflection point of the distance to the source of gradient of the sperm path prior to the first Ca^{2+} fluctuation; *max* the farthest point to the source of the gradient, and *min* indicates the nearest point to the source of the gradient. ϕ values were calculated at the beginning of the 200 ms UV flash ($\phi_{UV\ begin}$, Fig. S5), at the end of the 200 ms UV flash ($\phi_{UV\ end}$, Figs. 10A, B, E, and F), or at the beginning of the first Ca^{2+} fluctuation (ϕ_{F1}, Figs. 10C and G).

Statistical analyses

Data are presented from spermatozoa collected from a minimum of three sea urchins and all error bars represent standard error of the mean unless otherwise stated. Kolmogorov–Smirnov (differences in α or ϕ distributions) and Student's *t*-test (comparison of means) analyses were performed with GNU Octave software v3.0.1 and Microsoft Office Excel 2007; in some cases Bonferroni's correction was implemented (Fig. 6). To test the bias in the frequencies of two mutually exclusive events, such as the percent of Ca^{2+} fluctuations of Type $(-)$ vs. Type $(+)$, a Binomial test was performed using R software v. 2.7.1. Data that do not show normal distribution were analyzed with the Wilcoxon rank sum test using R software v. 2.7.1. The statistical significance level was set at 95% or 99% as indicated in the main text.

Results

The spermatozoa motility response to speract

We examined the swimming pattern of spermatozoa in a speract gradient established by a 200 ms pulse of UV light whose profile was derived from the spatial distribution of the light scattered at the glass–liquid interface (Fig. 1). Fluo-4 loaded *L. pictus* and *S. purpuratus* spermatozoa were placed into separate chambers filled with artificial sea water (ASW) containing 10 nM of caged speract that has a receptor binding affinity approximately 1400× lower than native speract (caged speract IC50 = 950 nM vs. 0.66 nM for native speract).

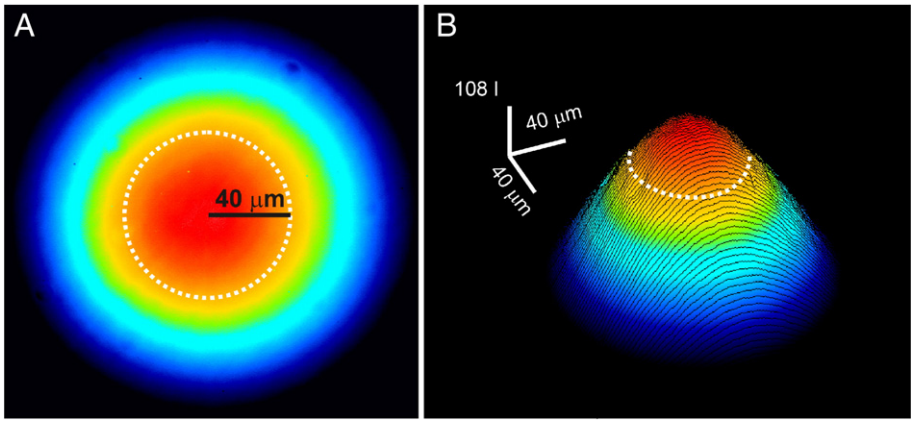

Fig. 1. UV flash energy spatial distribution. A) UV light scattered at the glass–liquid interface generated via an optical fiber coupled to a xenon lamp. A pseudo-color scale representing maximum (red) and minimum (blue) relative light intensities was used. B) Surface plot of (A) illustrating the shape of the UV light generated gradient where the *I-axis* represents the relative light intensity distribution.

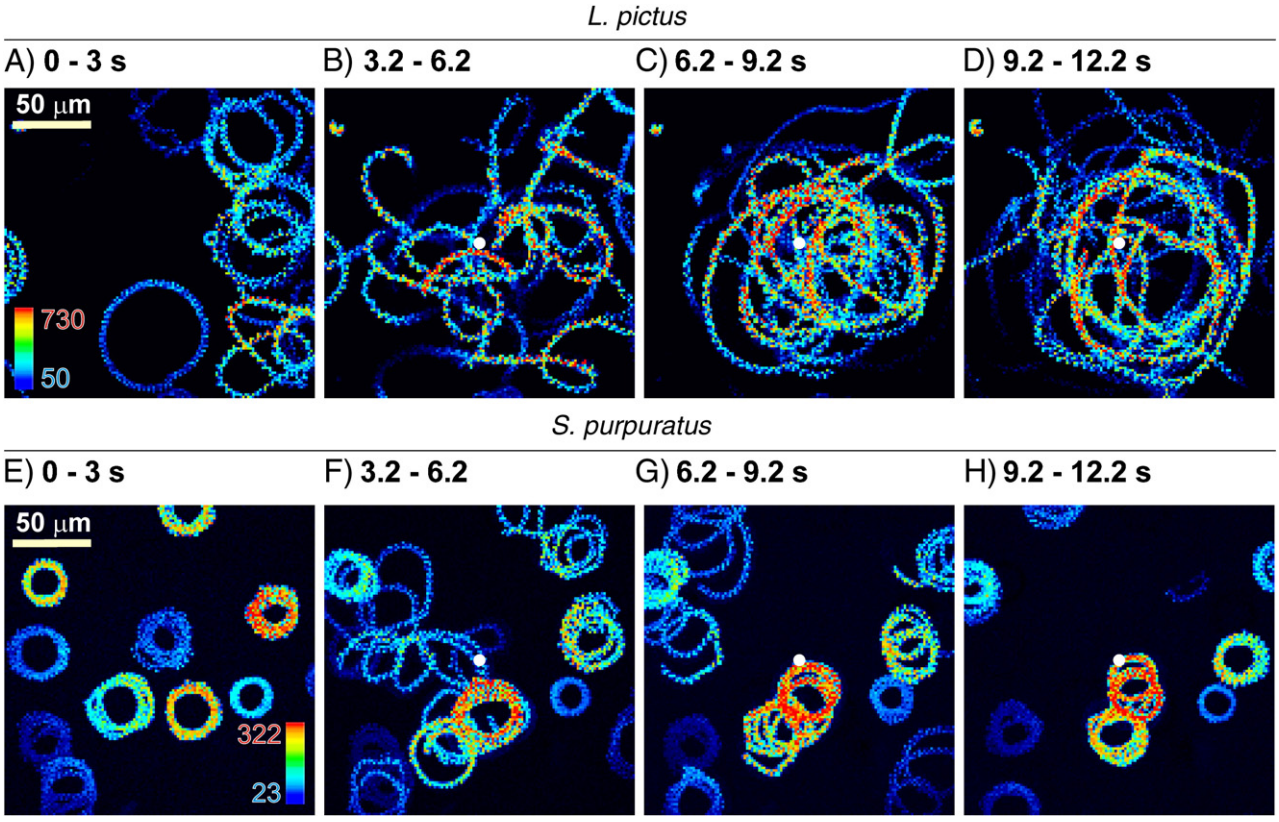

Fig. 2. Typical speract-induced motility changes of *L. pictus* and *S. purpuratus* spermatozoa. A–D) *L. pictus* spermatozoa motility response to speract. E–H) *S. purpuratus* spermatozoa motility response to speract. F–F0 time projections showing spermatozoa head fluorescence 3 s before (A, E) and 3 s (B, F), 6 s (C, G) and 9 s (D, H) after 200 ms UV photoactivation of 10 nM caged speract in ASW. The white dot shows the center of the irradiated area.

Figs. 2A and E show thigmotactic circular swimming behavior of unstimulated *L. pictus* and *S. purpuratus* spermatozoa at the glass–water interface: average radius of 24.9 ± 1.0 μm (*L. pictus*, 1.67 revolutions s^{-1}) and 17.8 ± 1.0 μm (*S. purpuratus*, 1.45 revolutions s^{-1}). Only the fluorescent signal from the head could be recorded in unstimulated spermatozoa, as found previously. After irradiation spermatozoa of both species deviated from the path of their prior circular trajectory through an alternating sequence of turns interspersed with periods of straighter swimming, the turn-and-run pattern (Figs. 2B and F). This stereotypical motility response is seen in spermatozoa of diverse marine species upon exposure to components of the homologous egg.

During the initial phase of the motility response the *L. pictus* spermatozoa accumulated at the center of the irradiated area, the zone that contains the highest concentration of speract (Fig. 2B, Movie S1). This initial motility response lasted for ~3 s following irradiation, after which the spermatozoa swam in circles surrounding the center of the field (Fig. 2C). The average radius of these circles was greater than those observed prior to speract uncaging: 62.5 ± 7.7 μm at 9 s after stimulation, $p<0.01$, *t*-test (Fig. 2D). In contrast, *S. purpuratus* spermatozoa did not accumulate at the center of the irradiated area, or at any other point in the recording field (Figs. 2E–H, Movie S2), despite undergoing a similar sequence of initial motility changes to those seen in *L. pictus* spermatozoa (Fig. 2F).

Single cell speract-induced motor responses

Single cell trajectories were tracked by following the head centroid. After uncaging speract, spermatozoa swam along their original path for hundreds of milliseconds before initiating the switch to the 'turn-and-run' pattern. This change coincided with transient alterations to the flagellar waveform (Fig. 3). The trajectory of a *L. pictus* spermatozoon is shown in Fig. 3A from 3 s before (black trace) to 9 s after irradiation (red trace). Below, an excerpt shows the trajectory during a single turn-and-run episode, where a black dot indicates the beginning of the first increase in flagellar fluo-4 fluorescence (Figs. 3A and B). The average delay after the 200 ms of UV exposure to the onset of the first Ca^{2+} fluctuation was 371 ± 81 ms for *L. pictus* ($n=13$) and 247 ± 27 ms ($n=15$) for *S. purpuratus* spermatozoa. Turning episodes coincided with an increase in flagellar fluorescence and a transient alteration in flagellar waveform characterized by strong bending of the proximal portion and extension of the distal portion of the flagellum (Fig. 3B). This response was followed by a period of almost straight swimming. This behavior is represented as changes in the local path curvature ($1/r$ (μm^{-1})) of the swimming trajectory; after stimulation, the curvature first steeply increased and then decreased below baseline values (Fig. 3B). Increases in $[Ca^{2+}]_i$ and path curvature changes were not proportionately related (Fig. 3B), as reported previously in *S. purpuratus* spermatozoa (Darszon et al., 2008; Wood et al., 2007). We were unable to record the complete duration of the Ca^{2+} fluctuations in *L. pictus* spermatozoa, as during the Ca^{2+}-decreasing phase the spermatozoa transiently swam out of the plane of focus. Hence the shaded yellow area in Fig. 3A marks only the recordable duration of the Ca^{2+} fluctuation, and terminates once the spermatozoon temporarily left the focus plane.

The speract-induced flagellar Ca^{2+} responses, and resultant flagellar curvature alterations, of *S. purpuratus* spermatozoa have

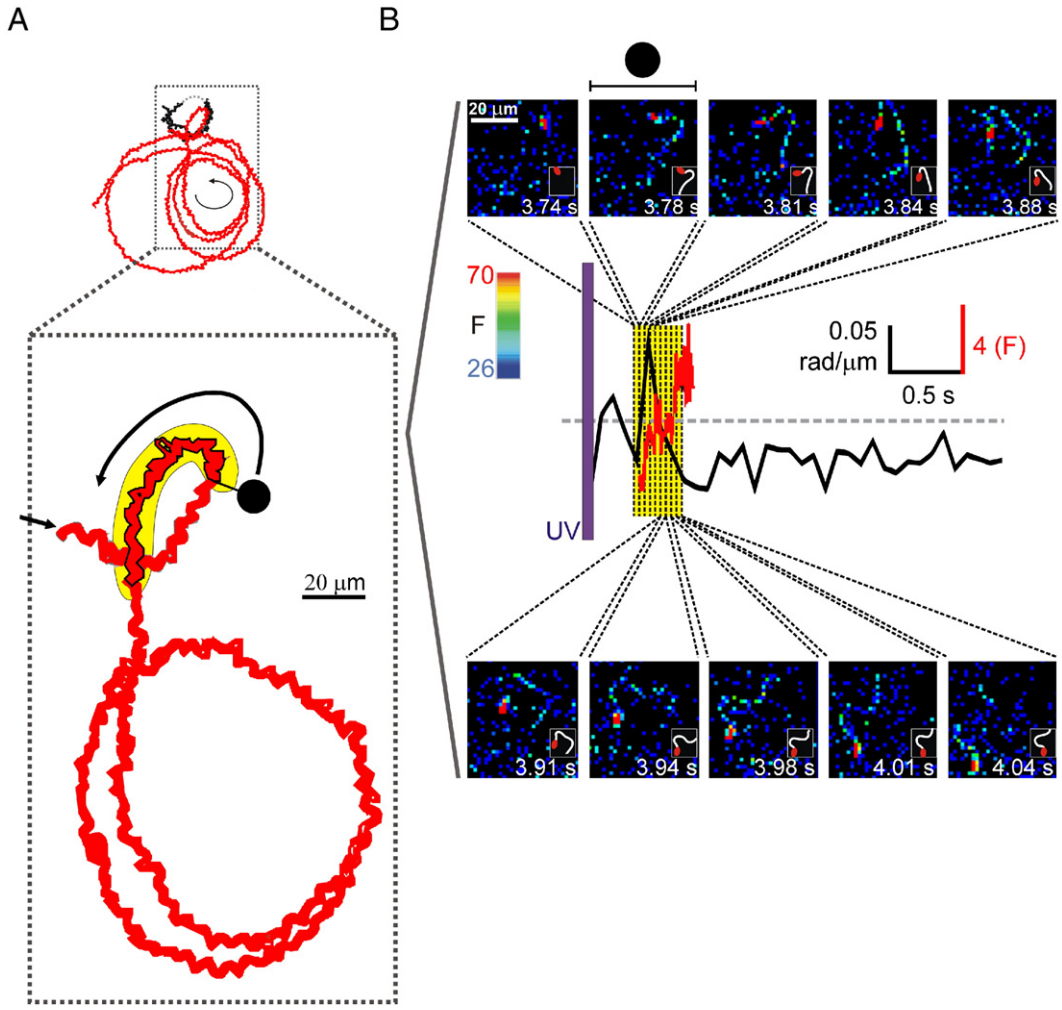

Fig. 3. Single turn-and-run swimming episode of a *L. pictus* spermatozoon generated by a transient flagellum $[Ca^{2+}]_i$ increase. A) Trajectory 3 s before (black trace) and 9 s after (red trace) speract stimulation. The box shows a single turn-and-run episode followed by two circles in the 3 s immediately after speract photoactivation. B) Intra-flagellum Ca^{2+} dynamics (red trace) and path curvature (black trace) changes experienced after speract exposure. Panels show images of a typical transient increase in fluo-4 fluorescence in the flagellum. A, B) A black dot was assigned at the time when the flagellum becomes visible and indicates the beginning of the first flagellum fluorescence increase. The yellow envelope depicts the time interval in which the spermatozoon flagellum was visible.

been reported previously, and the spermatozoa employed in the current study displayed essentially identical behavior (Darszon et al., 2008; Wood et al., 2007).

The speract-induced motor responses of L. pictus spermatozoa are shaped by the spatial distribution of the speract gradient

We observed that *L. pictus* spermatozoa displayed markedly dissimilar motility responses depending on their position relative to the source of the speract gradient. Based on this observation we defined two populations for further analysis: a proximal population (Proximal P.) that were initially located greater than 40 µm distant from the source of the speract gradient, and a central population (Central P.) that were inside this 40 µm limit. The response of an *L. pictus* spermatozoon of the Proximal P. to stimulation was typically biphasic (Figs. 4A–C, also see Figs. S1A–C). During the first phase, during the first 3–5 s following UV irradiation, Proximal P. spermatozoa re-localized towards the source of the speract gradient due to pronounced turns that occurred as the spermatozoa swim away from the center of the field (Figs. 4A and S1A; red bar in Figs. 4B and S1B, see also Fig. 2B). Each turn coincided with a transient flagellar Ca^{2+} increase (see: i–iv, Figs. 4A–C; and i–v, Figs. S1A–C) and was followed by a straight swimming period (Figs. 4C and S1C). The second phase of the response could be characterized by the general absence of turning events, and a gradual increase in the size of the circular spermatozoa swimming trajectory (Figs. 2C–D; green bar in Figs. 4B and S1B; Movie S2).

The motility response of the *L. pictus* Central P. spermatozoa in the speract gradient was markedly different during the initial phase. These spermatozoa do not show large lateral displacements in their swimming trajectory, but tend to remain at the center of the imaging field, despite initiating a sequence of Ca^{2+} fluctuations and coincident turning events (compare Figs. 4D–F and A–C; also compare Figs. S1D–F and A–C). As with the Proximal P., the initial phase of the response in Central P. spermatozoa was followed by a secondary phase marked by the general absence of Ca^{2+} fluctuations and turning events (green bar on Figs. 4D and S1D).

Typically, *S. purpuratus* spermatozoa underwent a speract-induced re-localization, driven by turn-and-run episodes that were triggered by flagellar Ca^{2+} fluctuations (Figs. 4G–I). We did not observe differences between *S. purpuratus* Central and Proximal populations, nor a biased re-localization. As with *L. pictus* spermatozoa, a secondary phase response was observed in which the 'turn-and-run' behavior diminished and eventually spermatozoa resumed their circular swimming trajectories, as before stimulation (Figs. 4G–I and 2E–H).

All speract-induced motor responses recorded, whether from *L. pictus* or *S. purpuratus* spermatozoa, were biphasic with the transient turn-and-run episodes superimposed on a sustained tonic decrease in

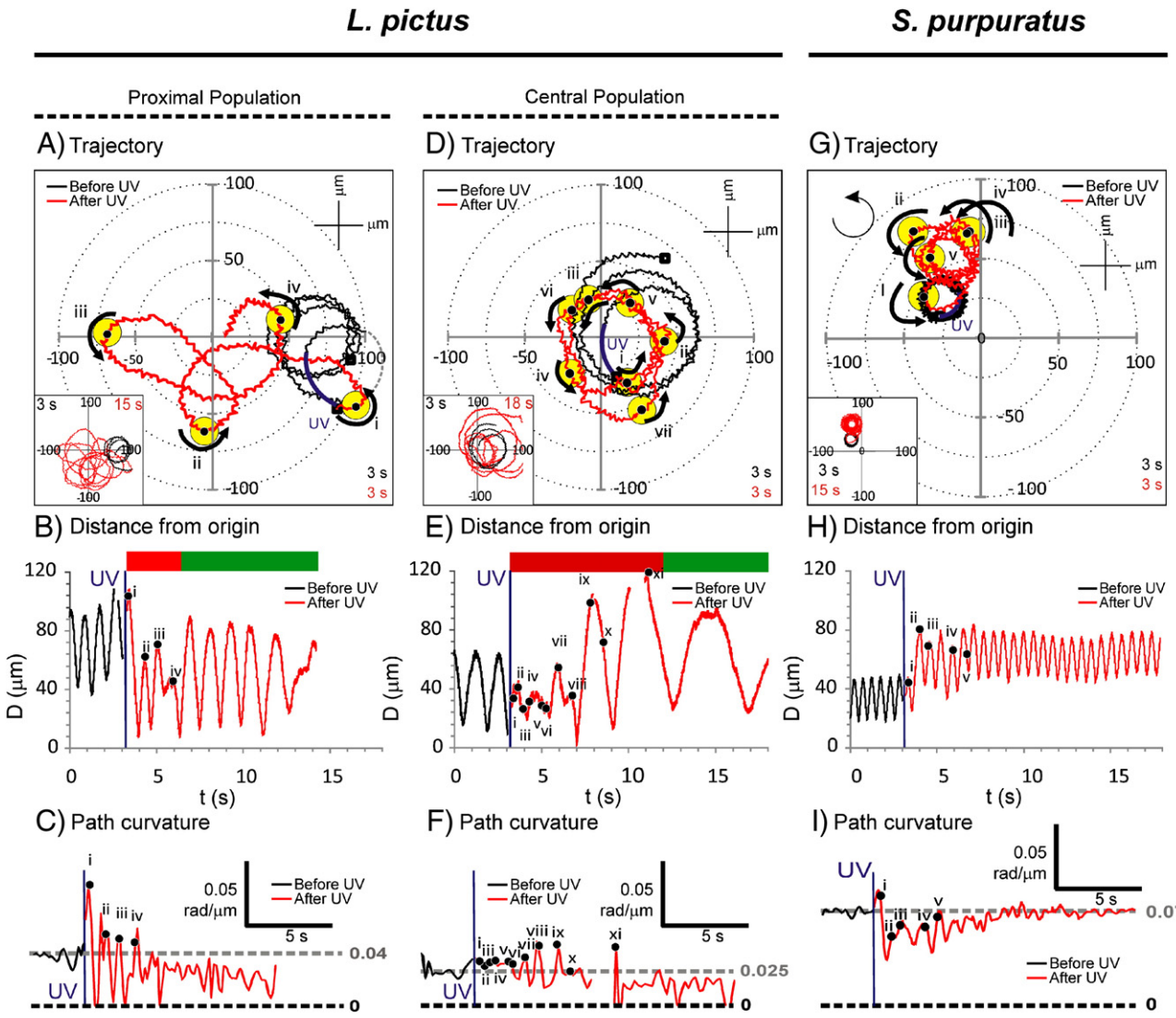

Fig. 4. Speract photoactivation induces characteristic motility changes in single spermatozoa. Single cell trajectories 3 s before (black traces) and 3 s after (red traces) speract stimulation of *L. pictus* spermatozoa from Proximal (A) or Central (D) populations; or of *S. purpuratus* spermatozoa (G). As no clear differences between Proximal and Central populations were seen in *S. purpuratus*, only one example is presented. Inserts show motility behavior 3 s before (black) and 12–15 s after (red) stimulation. B, E, H) Spermatozoa head distance to the source of the speract gradient vs. time calculated from trajectories of A, D and G, respectively. Color bars (red, green) indicate the primary and secondary phase responses. C, F, I) Path curvature of the same spermatozoa shown in A, D and G; respectively. A–I) Black dots indicate spermatozoa position at the beginning of an individual Ca^{2+} fluctuation, roman numerals mark sequence: i–iv (A, B, C), i–xi (D, E, F), and i–v (G, H, I). For clarity in A, D and G each black dot is surrounded by a yellow circle. Other experimental conditions as in Fig. 2. Purple bars indicate a 200 ms UV photoactivation of speract.

curvature which was more pronounced in spermatozoa from *L. pictus* (Figs. 4C, F, I and S1C and F). In zero Ca^{2+} ASW the speract-induced spermatozoa motility response was monophasic, consisting solely of the tonic curvature decrease (Fig. S2). Hence only the speract-induced turn-and-run responses require extracellular Ca^{2+}.

Analysis of spermatozoa chemotaxis

To ascertain whether the motility changes recorded for *L. pictus* and/or *S. purpuratus* constitute a bona fide chemotactic response we employed the LECI analysis originally devised for analyzing ascidian spermatozoa motility (Yoshida et al., 2002). LECI is defined as the negative value of the slope of a least square linear regression of the sperm head distance to the source of the chemoattractant gradient (D) vs. time (t) (Fig. 5A). Figs. 5B and C show the least square linear regressions for the paths traced by *L. pictus* spermatozoa of Proximal and Central populations 3 s after speract stimulation, respectively. Several time windows (3, 6 and 9 s after speract stimulation) were tested to find the best time interval for the assessment of a chemotactic response (Fig. 6).

As Proximal P. *L. pictus* spermatozoa approached the source of the speract gradient, D decreased with periodic oscillations during the first 3 s after speract stimulation (Fig. 5B). This continuous decrease gave a positive LECI (13.09 ± 2.32 µm/s) that was significantly different ($p<0.001$, t-test with Bonferroni's correction) from the control condition (-2.18 ± 1.25 µm/s, 3 s before stimulation), indicating that the re-localization of Proximal P. *L. pictus* spermatozoa was due to a chemotactic motility response (Fig. 6). LECI windows of 6 s or 9 s gave near-zero values (-0.05 ± 1.21 µm/s ($p=0.30$) and -1.02 ± 0.88 µm/s ($p=0.56$), respectively) (Fig. 6). In spermatozoa of the *L. pictus* Central P., LECIs (3, 6 or 9 s windows) were not significantly different to controls (Figs. 6 and 5C). In *S. purpuratus* spermatozoa, none of the conditions analyzed (Proximal or Central populations; 3, 6 or 9 s time windows) gave positive LECIs significantly different from controls (Fig. 6). We also confirmed that the chemotactic motility response of *L. pictus* spermatozoa was blocked in zero Ca^{2+}

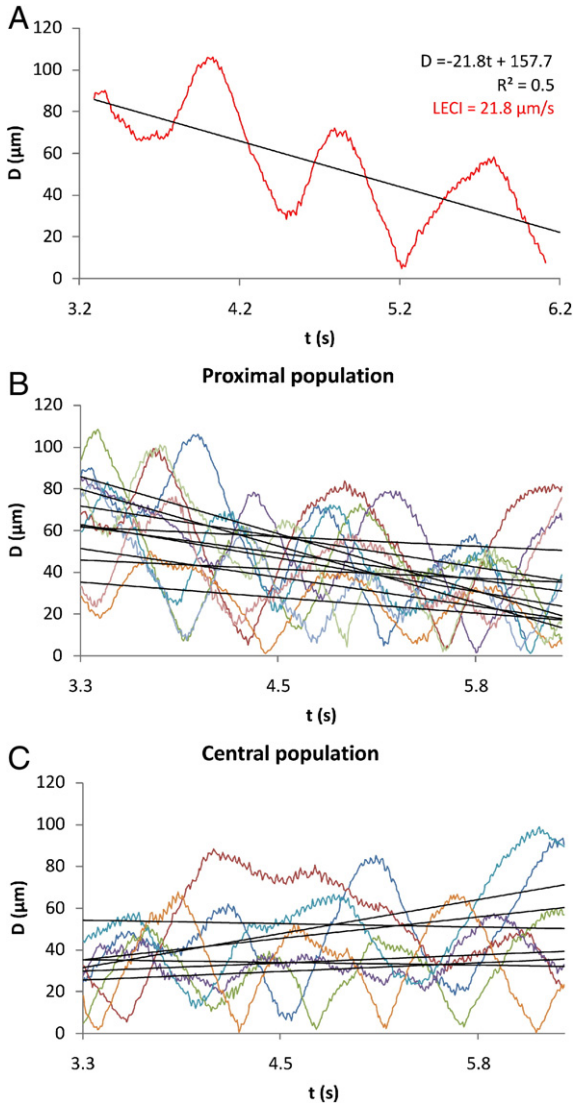

Fig. 5. Linear equation chemotaxis indices (LECI) quantitatively describe the spermatozoa motility behavior in a chemoattractant gradient. Least square linear regressions of *L. pictus* spermatozoa head distances to the source of the chemoattractant gradient vs. time 3 s after speract photoactivation. A, B) Proximal P. *L. pictus* spermatozoa approaching the speract gradient origin. C) Central P. *L. pictus* spermatozoa demonstrating a non-biased re-localization.

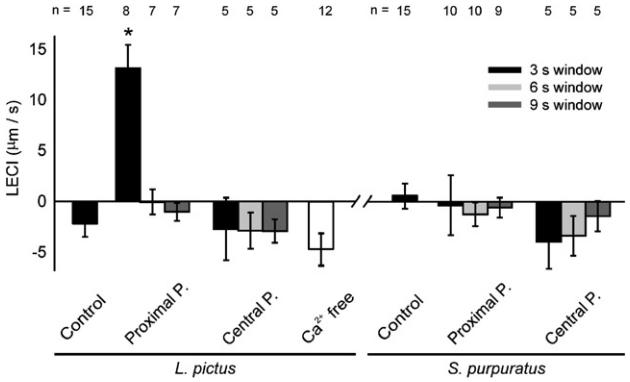

Fig. 6. Speract chemotaxis is spatiotemporally restricted. LECIs calculated for *L. pictus* (left panel) or *S. purpuratus* spermatozoa (right panel) using 3, 6 and 9 s temporal windows (black, pale and dark gray bars, respectively). Control: Before UV photoactivation; Proximal P: Proximal spermatozoa population: Central P: Central spermatozoa population: Ca^{2+} free: *L. pictus* spermatozoa swimming in free Ca^{2+} ASW containing 10 nM caged speract 3 s after UV irradiation (white bar). Other experimental conditions as in Fig. 2. * Pair-wise comparisons against respective control condition using *t*-test with Bonferroni's correction ($p<0.001$). Error bars = SE.

ASW (Fig. 6) due to the absence of speract-induced Ca^{2+} fluctuations in the sperm flagella (Fig. S2, Movie S3).

We next considered if the positive LECI calculations for Proximal P. spermatozoa could in fact represent a selection bias for spermatozoa that swam towards the center of the field — due to limitations in the field of view (~200×200 µm) Proximal P. spermatozoa that swam away from the center would rapidly exit this field and be excluded from the sampled population. To investigate this possibility we visualized the response of speract-stimulated *L. pictus* spermatozoa within a larger field of view using a 20× objective (~400×400 µm) (Movie S4). As the UV field is generated by projection through the back-plane of the objective, an optical fiber of reduced terminal aperture was employed to ensure approximate consistency between the absolute diameter and shape of the speract gradient generated using the 20× and 40× objectives (shown in Fig. S3B). The paths of individual spermatozoa across the entire field are displayed in Fig. S3C. Proximal and Central P. spermatozoa were clearly identified (Figs. S3E and F) and an unresponsive third population was found at >170 µm from the source of the speract gradient (Distal P., Fig. S3D). LECIs calculated for each spermatozoon are presented in Table S1 according to their Distal, Proximal or Central classification. Only Proximal P. *L. pictus* spermatozoa gave a positive averaged LECI (µm s^{-1}: Distal P. = 3.8 ± 4.0, Proximal P. = 16.9 ± 4.0, Central P. = 0.6 ± 1.8).

Sperm chemotaxis is tuned by the timing of flagellar Ca^{2+} fluctuations

As spermatozoa swim in a speract gradient, they continuously experience changes in the rate of stimulation due to speract binding (the stimulus function). When a spermatozoon swims up a chemoattractant gradient (towards the source) the stimulus function increases as *D* decreases, and conversely, when the spermatozoon is swimming down the gradient (away from the source), the stimulus function decreases as *D* increases. There is evidence showing that the stimulus function of *A. punctulata* spermatozoa and their flagellar Ca^{2+} fluctuations are synchronized (Bohmer et al., 2005), therefore we decided to investigate if this synchronization determines chemotactic behavior in sea urchin spermatozoa. The direction of individual *L. pictus* or *S. purpuratus* spermatozoa was determined at the beginning of each Ca^{2+} fluctuation by measuring the angle (α) formed between the vectors that define sperm position (***P***-vector) and direction (***R***-vector) in relation to the source of the speract gradient (Fig. 7A). An α value between 0 and 90° identifies Ca^{2+} fluctuations initiating in a negative speract concentration gradient (Type (−) Ca^{2+} fluctuation), while α values between 90 and 180° indicates that the spermatozoon was swimming up a positive speract concentration gradient (Type (+) Ca^{2+} fluctuation); upper and lower panel of Fig. 7A, respectively.

We next examined the distribution of Type (+) and Type (−) Ca^{2+} fluctuations in *L. pictus* spermatozoa. Our null hypothesis was that there is no relationship between the speract stimulus function and the position of the spermatozoa in relation to the direction of the speract gradient, which would manifest as an equal and unbiased distribution of Type (−) and Type (+) Ca^{2+} fluctuations with respect to α values between 0 and 180°. As seen in the left panel of Fig. 7B, *L. pictus* spermatozoa of the chemotactic Proximal population display a skewed distribution of α values towards the 0–90° range, indicating a preference to undergo Type (−) Ca^{2+} fluctuations (87% $_{\text{Type (−)}}$: 13% $_{\text{Type (+)}}$ (Fig. 8A, Movie 5). The former distribution deviated from a theoretically expected distribution with 50% probability for Type (−) or Type (+) Ca^{2+} fluctuations ($p<0.01$, binomial test). We found that 81.3% of Type (−) Ca^{2+} fluctuations exhibited by *L. pictus* spermatozoa of Proximal population occurred close to the point of maximum distance to the source of the gradient.

Spermatozoa of the central population showed a diminished preference for Type (−) Ca^{2+} fluctuations (63% $_{\text{Type (−)}}$: 37% $_{\text{Type (+)}}$,

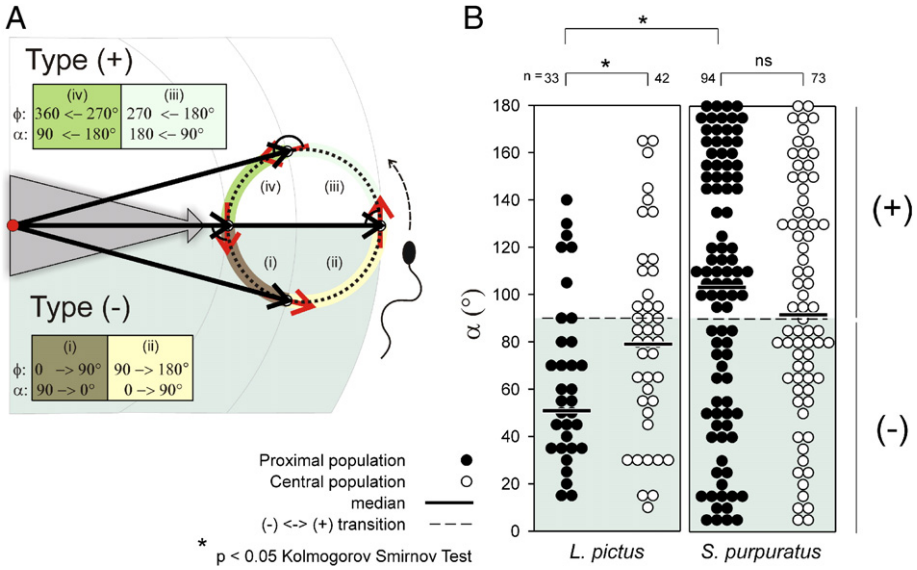

Fig. 7. *L. pictus* spermatozoa preferentially evoke Ca^{2+} fluctuations when swimming down the speract gradient. A) Speract-induced Ca^{2+} fluctuations were classified as Type (−) or Type (+) according to the angle α or ϕ formed between ***P*** and ***R*** vectors (black and red arrows respectively) of the spermatozoa swimming direction in relation to the speract gradient source. The red circle indicates the source of speract gradient and the gray shadowed arrow its direction. The roman numerals mark α or ϕ quadrants corresponding to a negative (i–ii) or positive (iii–iv) gradient. B) Distributions of α values for *L. pictus* (left panel) and *S. purpuratus* (right panel) spermatozoa. Only *L. pictus* spermatozoa display a biased distribution of α values in the 0–90° range indicating a preference to undergo Type (−) Ca^{2+} fluctuations.

median = 79.0°) with no significant deviation from a theoretically expected 50% probability distribution for both types of Ca^{2+} fluctuations ($p = 0.2$, binomial test) (Fig. 8A). The distribution of the Proximal and Central P. *L. pictus* spermatozoa α values was significantly different ($p < 0.05$, Kolmogorov–Smirnov test) (Fig. 7B, left panel).

The distribution of α values for *S. purpuratus* Proximal P. and Central P. spermatozoa shows no preference towards the 0–90° vs. 90–180° range (median = 103.4°), and there was no statistically significant difference between the two populations (Fig. 7B, right panel, α value median = 91.9° ($p = 0.3$, Kolmogorov–Smirnov test)).

We found a clear difference in α distribution between Proximal populations of *L. pictus* and *S. purpuratus* spermatozoa ($p < 0.01$, Kolmogorov–Smirnov test) strongly suggesting that a tendency to undergo Type (−) Ca^{2+} fluctuations is a requirement for the development of a chemotactic response (Fig. 7B).

L. pictus but not S. purpuratus spermatozoa have a mechanism to block Type (+) Ca^{2+} fluctuations that operates during the initial phase of the speract response

Studies with immobilized *S. purpuratus* spermatozoa show that the frequency of the speract-induced flagellar Ca^{2+} fluctuations is dose-dependent (Wood et al., 2003). We found that in the presence of a speract gradient, the *L. pictus* Central P. spermatozoa generate a greater average total number of flagellar Ca^{2+} fluctuations than the Proximal P. (Fig. 8B: $n_{\text{Central P.}} = 8.8 \pm 1.4$ and $n_{\text{Proximal P.}} = 4.1 \pm 0.7$ ($p < 0.05$, *t*-test)). This suggests that the number of Ca^{2+} fluctuations in speract-stimulated *L. pictus* spermatozoa is sensitive to the absolute initial concentration of speract and/or to the form and steepness of the speract gradient. During UV irradiation Central P. spermatozoa would experience a steeper temporal gradient than spermatozoa of the Proximal P., as the step change in speract concentration is greater at the center of the UV illumination field.

In *S. purpuratus* spermatozoa there was no significant difference between the total number of Ca^{2+} fluctuations generated by the proximal and central populations (Fig. 8E). Comparing between species, the number of Ca^{2+} fluctuations experienced by *S. purpuratus* and *L. pictus* Central P. spermatozoa was broadly similar (Figs. 8B and E: $p = 0.38$, *t*-test; gray bars), although their respective Proximal populations differed significantly, with those of *S. purpuratus* demonstrating a greater number of Ca^{2+} fluctuations (Figs. 8B and E). This difference was largely due to a relatively low number of Type (+) Ca^{2+} fluctuations in the *L. pictus* Proximal sperm population (Figs. 8B and E), indicating that spermatozoa from this species have a mechanism to block Type (+) Ca^{2+} fluctuations (compare only Type (+) condition between Proximal P. of *L. pictus* vs. *S. purpuratus* spermatozoa; Figs. 8B and E, black bars).

That the *L. pictus* Proximal P. is the only sperm population tested here to clearly demonstrate chemotactic motility responses strongly suggests that an apparent preference for Type (−) Ca^{2+} fluctuations over Type (+) Ca^{2+} fluctuations may underlie the chemotactic mechanism. If so, as chemotactic motility changes in the *L. pictus* Proximal P. are largely restricted to the initial phase of the motility response, we examined whether the preference for Type (−) Ca^{2+} fluctuations was similarly temporally confined. Type (+) Ca^{2+} fluctuations did not appear in the *L. pictus* Proximal P. until ~3 s after the UV stimulation (Figs. 8C and 9A), which correlates with the transition from the initial (chemotactic) phase of the response to the secondary phase. In all other populations examined (*L. pictus* Central P.; *S. purpuratus* Central and Proximal P. Figs. 8C, F, 9B–D, and S4) the Type (+) Ca^{2+} fluctuations appeared immediately after the UV stimulation and occurred simultaneously with Type (−) Ca^{2+} fluctuations. This suggests that the suppression of Type (+) Ca^{2+} fluctuations during the initial phase of the motility response to speract is a distinguishing feature of chemotactic motility in sea urchin spermatozoa.

The delay between speract binding and the onset of the first Ca^{2+} increase is regulated by the shape of chemoattractant gradient

We next investigated whether the mechanism to suppress Ca^{2+} fluctuations in a positive speract gradient in *L. pictus* spermatozoa is robust enough to adapt to differing forms and durations of chemoattractant gradient by analyzing in greater detail the behavior of sperm during the period between the UV uncaging event and the first Ca^{2+} fluctuation. In these conditions, the duration of exposure to an ascending speract gradient in each sperm will depend on its position at the end of the period of UV exposure. Initially, increases in speract concentration created during the 200 ms exposure to UV light will be sensed by all spermatozoa in the field as a positive gradient of

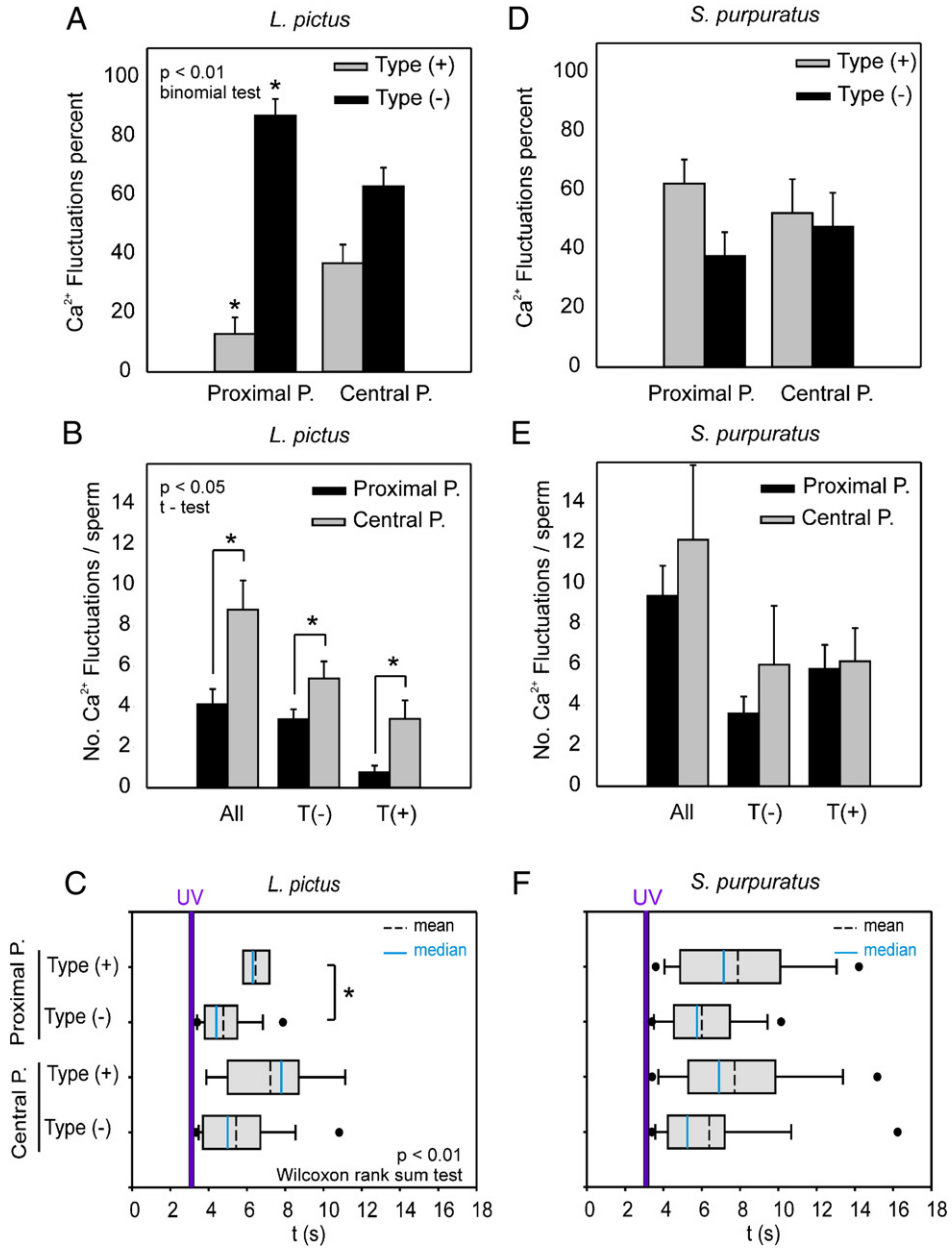

Fig. 8. *L. pictus* and *S. purpuratus* spermatozoa differentially regulate their Type (−) and Type (+) Ca^{2+} fluctuations. A, D) Percent of Ca^{2+} fluctuations in *L. pictus* (A) and *S. purpuratus* (D) Proximal and Central sperm populations. B, E) Total number of Ca^{2+} fluctuations/spermatozoa in *L. pictus* (B) and *S. purpuratus* (E): T(−) = Type (−), T(+) = Type (+), and All = Type (−) + Type (+). At least 9 spermatozoa from at least 3 different sperm batches were used for each condition of Proximal P. for both *L. pictus* or *S. purpuratus* species, and at least 6 was used for Central P. conditions, Error bars = SE. C, F) Box plots showing the time dependence of Ca^{2+} fluctuations exhibited by Proximal (upper section) and Central (lower section) populations of *L. pictus* (C) and *S. purpuratus* spermatozoa (F). The boundaries of the boxes indicate the 25–75th percentile range. Solid line = median value and broken line = mean value. Error bars above and below the boxes indicate the 90th and 10th percentiles.

speract. At the end of the 200 ms UV exposure the newly-formed chemoattractant gradient is essentially static over the timescale of the delay to the first Ca^{2+} fluctuation, and spermatozoa will find themselves in either a newly-formed positive or negative gradient. If the mechanism to suppress Ca^{2+} fluctuations in ascending chemoattractant gradients is robust, then the two populations of sperm (ascending gradient after UV, or UV_{pos}, and negative gradient after UV, or UV_{neg}) should differ in the delay they experience before undergoing the first Ca^{2+} fluctuation.

Spermatozoa of the UV_{neg} population experience an immediate chemoattractant gradient inversion from ascending to descending at the end of the UV exposure, instantaneously initiating the signaling cascade that triggers the Ca^{2+} fluctuation and flagellar motility changes. Sperm of the UV_{pos} population, however, will initially swim within a continuing ascending speract gradient, experiencing a relative delay before reaching the gradient inversion point at which the chemotactic turn-promoting signaling mechanism is activated. Thus we predict that UV_{pos} sperm will show significantly increased intervals between the end of the UV exposure and the initiation of the first Ca^{2+} fluctuation than sperm of the UV_{neg} population. The consequence of such robustness in the mechanism would be to preserve the bias in selectively generating Ca^{2+} fluctuations and chemotactic turns in negative speract gradients at the first Ca^{2+} fluctuation; one corollary would be that in *S. purpuratus* sperm, such bias should be absent, and delays to the first Ca^{2+} fluctuation should not differ between UV_{pos} and UV_{neg} populations in this species.

Firstly, we determined the direction of individual *L. pictus* or *S. purpuratus* spermatozoa at the end of UV irradiation using the ϕ

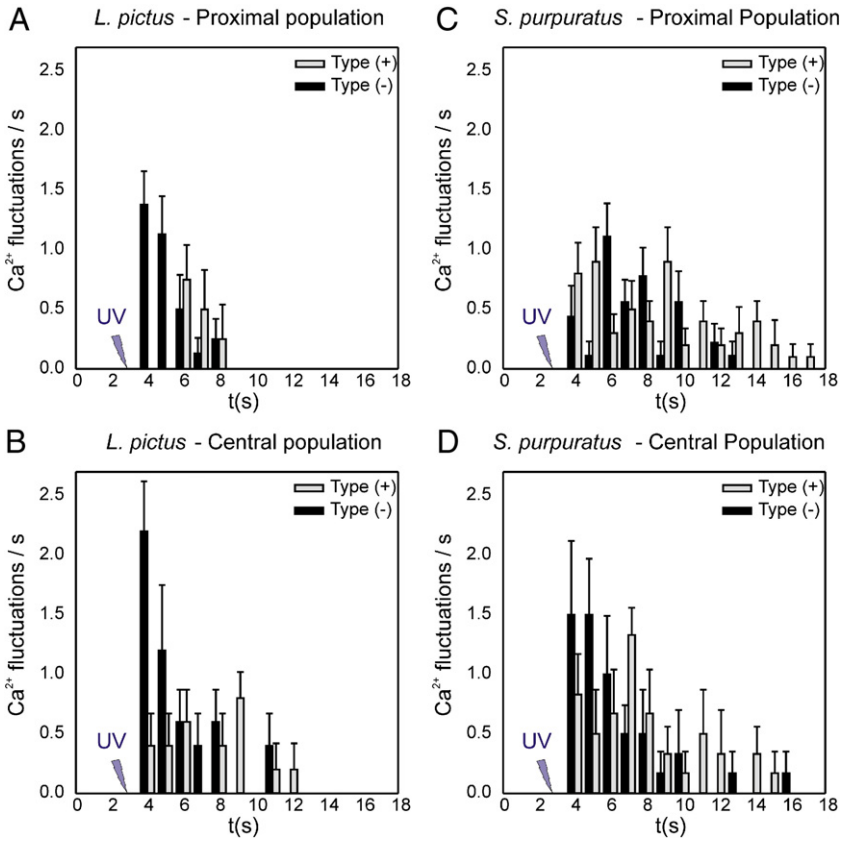

Fig. 9. Time dependence of the frequency of flagellar Ca^{2+} fluctuations. Number of Ca^{2+} fluctuations s^{-1} experienced after speract photoactivation of (A, B) *L. pictus* or (C, D) *S. purpuratus* spermatozoa. Proximal and Central populations are indicated, (A, C) and (B, D) respectively. Black bars: Type (−) Ca^{2+} fluctuations. Gray bars: Type (+) Ca^{2+} fluctuations. Experimental conditions as in Fig. 2. Error bars = SE.

angle (Fig. 7A), and correlated this value with the delay time required for the onset of the first Ca^{2+} fluctuation (Figs. 10A and E). Values of ϕ_{UVend} between 0 and 180° identify UV_{neg} spermatozoa, and ϕ_{UVend} values between 180 and 360° identify UV_{pos} spermatozoa. *L. pictus* Proximal P. spermatozoa of the UV_{pos} population significantly increased the average delay to the onset of the first Ca^{2+} fluctuation (410 ± 43 ms) compared to UV_{neg} spermatozoa (162 ± 10 ms); $p<0.001$, Wilcoxon rank sum test (Figs. 10A and B). Average delays to the first Ca^{2+} fluctuation in Central P. *L. pictus* spermatozoa of both UV_{pos} and UV_{neg} populations were similar to those of Proximal P. *L. pictus* UV_{neg} spermatozoa (171 ± 28 ms, 135 ± 12 ms, respectively; $p=0.4$, Wilcoxon rank sum test). In *S. purpuratus* sperm, average delay times for the onset of the first Ca^{2+} fluctuation of spermatozoa of UV_{pos} and UV_{neg} populations did not significantly differ; 388 ± 36 ms vs. 383 ± 43 ms, $p=0.9$, *t*-test (Fig. 10F).

As predicted, these data show that there was a relatively extended delay to the first Ca^{2+} fluctuation in *L. pictus* spermatozoa of Proximal P. that fell into a positive speract gradient at the end of the period of UV exposure, which was absent in *L. pictus* sperm of the Central P., and *S purpuratus* sperm under the same conditions.

But what of the functional consequences for chemotaxis of such an extended delay in UV_{pos} *L. pictus* sperm? We next examined whether this exaggerated delay was sufficient to retard the chemotactic turn until the sperm had entered the negative speract gradient. The position of individual *L. pictus* or *S. purpuratus* spermatozoa of Proximal P. at the beginning of the first Ca^{2+} fluctuation, relative to the direction of the speract gradient, was determined as before, but using the ϕ_{F1} angle (Fig. 7B), with Type (−) Ca^{2+} fluctuations and Type (+) Ca^{2+} fluctuations defined as previously (Fig. 7B). The distribution of the positions of *L. pictus* spermatozoa at the onset of the first Ca^{2+} fluctuations was skewed towards Type (−) Ca^{2+} fluctuations (66% Type (−) : 34% Type (+) $p<0.05$, binomial test) (Fig. 10C), whereas *S. purpuratus* spermatozoa show no significant deviation from a theoretically expected 50% probability distribution for both types of Ca^{2+} fluctuations (36% Type (−) : 64% Type (+), $p=0.07$, binomial test) (Fig. 10G). The initial positions immediately before stimulation (regarding (+) and (−) positioning in the gradient) were unbiased for all sperm subsets analyzed (Fig. S5). The data support the idea that the functional consequence of the extended delay seen in UV_{pos} spermatozoa of the *L. pictus* Proximal P. spermatozoa is to promote Type (−) Ca^{2+} fluctuations, which are a characteristic feature of chemotactic motility changes in *L. pictus* sperm.

There is evidence showing that the delay to initiate the Ca^{2+} increase in *A. punctulata* spermatozoa decreases from approximately 600 ms to 200 ms as the chemoattractant concentration increases from 10^{-13} to 10^{-9} M. No further increase in delay is seen at higher concentrations of chemoattractant (Kaupp et al., 2003). Fig. 10D shows that in UV_{pos} (but not UV_{neg}) *L. pictus* spermatozoa the delay varies according the proximity to the source of speract gradient (and thus absolute speract concentration). Under the same experimental conditions no *S. purpuratus* spermatozoa of either UV_{pos} or UV_{neg} showed a correlation between the delay times for the onset of the first Ca^{2+} increase and distance from the center of the UV field, indicating a diminished capability to detect the shape of speract gradient imposed (Fig. 10H).

Discussion

We have discovered that stimulation by a near-instantaneously generated gradient of the peptide speract induces chemotactic motility responses in sea urchin spermatozoa of *L. pictus* but not in spermatozoa of *S. purpuratus*. In both species the presence of a speract gradient triggers a train of Ca^{2+} fluctuations in sperm flagella that are

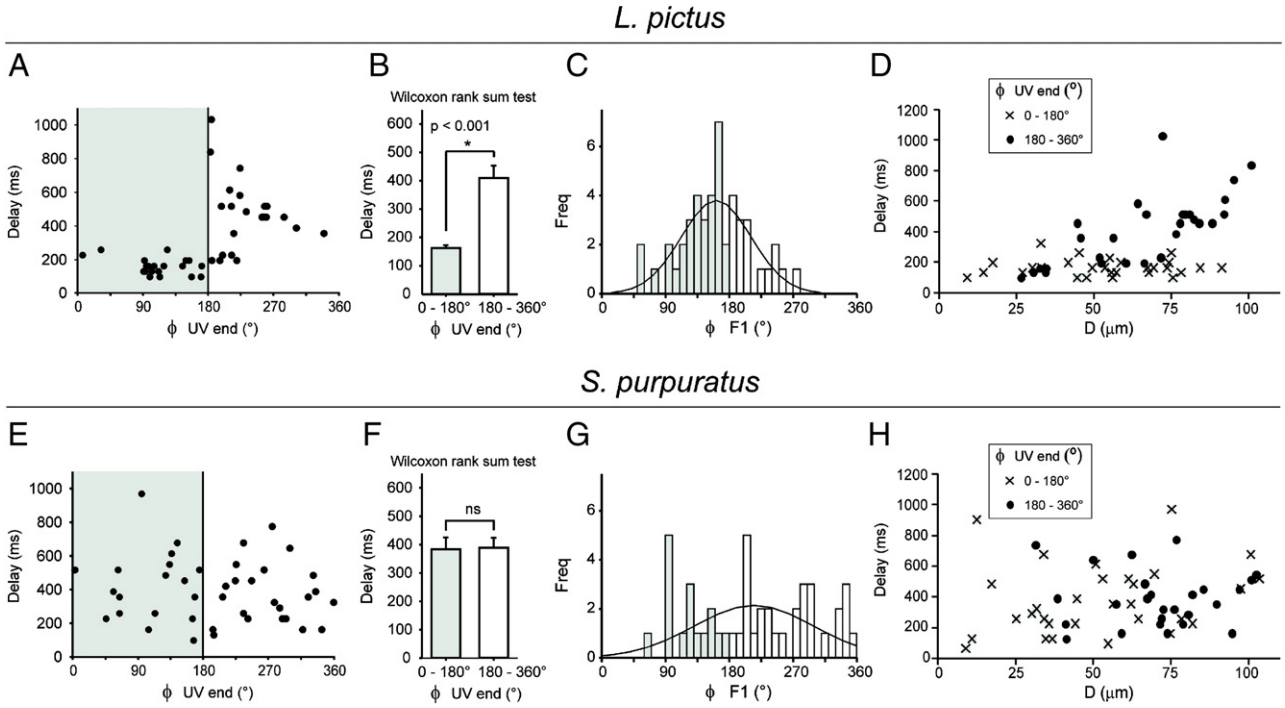

Fig. 10. *L. pictus*, but not *S. purpuratus*, spermatozoa retard the onset of the first Ca^{2+} fluctuation until reaching a descending phase of speract gradient. A, E) Relationship between spermatozoa position at the end of the 200 ms UV flash ($\phi_{UV\ end}$) and the delay time for the onset of the first Ca^{2+} fluctuation. B, F) Averaged delay for the onset of the first Ca^{2+} fluctuation of all spermatozoa that fall in a descending (left panel) or ascending (right panel) speract gradient at the end of the period of UV exposure. C, G) Distributions of ϕ values of the onset of the first Ca^{2+} fluctuation (ϕ_{F1}) for *L. pictus* (C) and *S. purpuratus* (G) spermatozoa. D, H) Dependence of the delay time for the onset of the first Ca^{2+} fluctuation with the distance to the source of speract gradient that fall in an ascending (dots) or descending (crosses) speract gradient at the end of the period of UV exposure for *L. pictus* (D) and *S. purpuratus* (H) spermatozoa. A–C) *L. pictus* spermatozoa of proximal population. E–G) *S. purpuratus* spermatozoa of proximal population.

associated with stereotypical turn-and-run episodes that drive re-localization (Darszon et al., 2008; Kaupp et al., 2007). Ample evidence exists that the Ca^{2+}-dependent turning episodes are essential elements of a chemotactic motility response, most notably the inviolable requirement for extracellular Ca^{2+} in all chemotactic spermatozoa studied, from bracken to mammals (Brokaw, 1974; Eisenbach and Giojalas, 2006; Miller, 1985a). The motility response patterns of the two species shared certain similarities, as each species showed a generally biphasic response to speract gradient exposure. The first phase spanned the first 3–5 s of exposure, and was marked by the generation of Ca^{2+} fluctuations and turn-and-run episodes. A second phase then followed, marked by larger diameter circular swimming trajectories, and by the general absence of Ca^{2+} fluctuations and turn-and-run motility alterations. The principal difference between *L. pictus* and *S. purpuratus* species was in the functional consequence of these sperm motility responses; only in the case *L. pictus* spermatozoa did they lead to chemotactic accumulation of spermatozoa at the source of the speract gradient, and of these, only of sperm of a proximal population located more than ~40 μm distant from the center. Thus the Ca^{2+}-dependent turning episodes and the interspersed periods of straighter swimming trajectories are necessary but not sufficient for chemotaxis, and the ability to undergo chemotaxis must lie in more subtle aspects of the timing of the turn-and-run pattern. Exploiting our ability to compare directly the motility responses of the two sea urchin species, we set out to uncover the basis for the differential responses to the same stimulus.

Spatial and temporal regulation of chemotactic turns

Our findings show that within the chemotactic window approximately 80% of all Ca^{2+} fluctuations of the Proximal P. *L. pictus* spermatozoa occur while swimming down a negative speract gradient (defined as Type (−)), (Fig. 7B, left panel, and 10C). In contrast, *S. purpuratus* non-chemotactic spermatozoa generate Ca^{2+} fluctuations in both descending and ascending speract gradients. This suggests that Ca^{2+} fluctuations that occur in an ascending chemoattractant gradient (defined as Type (+)) do not favor chemotaxis, and conversely, selectively undergoing Type (−) Ca^{2+} fluctuations is a feature of chemotactic motility responses. Consistent with this observation, the periodic changes in chemoattractant concentration and Ca^{2+} fluctuations were shown to be synchronized in *A. punctulata* spermatozoa (Bohmer et al., 2005). Also a recent study demonstrated that *Ciona intestinalis* spermatozoa evoke Ca^{2+} fluctuations as the spermatozoa encounter chemoattractant gradient minima (Shiba et al., 2008). However, in neither of these studies was a synthesis of both the spatial and temporal aspects of chemotactic motility regulation presented.

As spermatozoa swim in a chemoattractant gradient they continuously sample the concentration field. The rate of binding of chemoattractant is a stochastic process that depends on sperm velocity and the direction of movement relative to the chemoattractant gradient. It was proposed that sperm $[Ca^{2+}]_i$ may increase when bound chemoattractants dissociate from the receptors once the spermatozoon enters a negative gradient (Miller, 1985a). This seems unlikely for speract since it is not expected to rapidly dissociate from its receptor ($k_{off} \sim 10^{-4}$ to $10^{-6}\ s^{-1}$), therefore, receptor occupancy is essentially unaltered while spermatozoa swim down-gradient (Nishigaki and Darszon, 2000; Nishigaki et al., 2001). The latter observation indicates that marine spermatozoa register relative, and not absolute, changes in chemoattractant concentrations, as has been previously suggested (Bohmer et al., 2005; Kaupp et al., 2003; Nishigaki et al., 2001; Shiba et al., 2008). It follows that spermatozoa experience the greatest relative change in chemoattractant concentrations at the points of transition between positive and negative speract gradients, which for a sperm swimming in a circular trajectory in a stationary gradient occur at the position closest to (positive to negative) and furthest from (negative to positive) the gradient source. Given the tendency for sperm undergoing chemotaxis to favor Type

(−) Ca^{2+} fluctuations, it is likely that the spermatozoa are sensitive to the positive-to-negative gradient inflection which when crossed, initiates the sequence of signaling events that produces the flagellar Ca^{2+} fluctuation and chemotactic turning event.

To test this idea, we examined the relationship between the position of the Ca^{2+} fluctuation (and chemotactic turn) and the preceding gradient inflection. We found that preference to undergo Type (−) Ca^{2+} fluctuations of *L. pictus* spermatozoa is due to their ability to suppress Ca^{2+} fluctuations while swimming along an ascending chemoattractant gradient (Figs. 10A and C). This tendency was best illustrated by examining the behavior of spermatozoa of the *L. pictus* spermatozoa Proximal P. immediately after the period of UV illumination. We found that spermatozoa which enter a positive speract gradient (UV_{pos}) will retard the onset of their first Ca^{2+} fluctuation approximately 400 ms, whereas for spermatozoa that enter a descending gradient (UV_{neg}) this delay is reduced to ~200 ms (see Figs. 10A and B). This extended delay in the UV_{pos} population probably represents the time required for the spermatozoa to reach the point of transition between ascending and descending speract gradients; in UV_{neg} sperm this point is reached immediately upon termination of the UV flash. The residual ~200 ms interval in the UV_{neg} population delay is probably close to the minimum time needed for the signal transduction events that lead to opening of the Ca^{2+} entry pathway (Kaupp et al., 2003; Nishigaki et al., 2004, 2001), which could comprise a cycle of hyperpolarization/depolarization leading to opening of Cav channels (Strunker et al., 2006).

For all subsequent Ca^{2+} fluctuations occurring after the first, the maximum decrease in the rate of speract binding occurs when they traverse from a positive to a negative gradient. For Proximal P. *L. pictus* spermatozoa during the 3 s chemotactic window the average delay from crossing this gradient inflection prior to each Ca^{2+} fluctuation was 220 ± 32 ms, similar to the value recorded for the same population of sperm that fall in the UV_{neg} population at the first Ca^{2+} fluctuation, and to the minimum post-stimulation delay reported in previous studies in spermatozoa of other sea urchin species (Kaupp et al., 2003; Nishigaki et al., 2004, 2001; Strunker et al., 2006). As a typical *L. pictus* spermatozoon swimming at 265 μm s^{-1} with a circular trajectory of 25 μm average radius and a circumference of 157 μm travels 1.69 revolutions s^{-1}, this delay would locate the chemotactic turns to a point close to the furthest distance from the source of the gradient. We observed just such a spatial distribution, with 81.3% of all measured Type (−) Ca^{2+} fluctuations of the Proximal P. *L. pictus* spermatozoa experienced during the "chemotactic window" occurring close to the point of maximum distance to the source of the gradient.

We therefore propose that the ability to selectively inhibit flagellar Ca^{2+} increases while experiencing an ascending chemoattractant gradient is an essential component that characterizes chemotaxis in sea urchin spermatozoa, and possibly chemotactic sperm motility in general.

A model for the molecular mechanism of sperm chemotaxis

In 1994, Cook et al. proposed that shallow or decreasing chemoattractant gradients elevate $[Ca^{2+}]_i$ to generate chemotactic turns, yet sufficiently steep increasing gradients maintain $[Ca^{2+}]_i$ low and swimming trajectories linear until the egg is reached (Cook et al., 1994). At the heart of the model lies a negative-feedback loop, in which SAP receptor binding activates guanylyl cyclase to elevate cGMP, which leads to a hyperpolarization of membrane potential due to cGMP-mediated activation of sperm K^+ channels (Bonigk et al., 2009; Galindo et al., 2000, 2007; Strunker et al., 2006). Subsequent inactivation of guanylyl cyclase and reduced cGMP levels terminate the hyperpolarizing conditions, leading to repolarization of membrane potential and opening of T-type Ca_v channels. In this model, chemotaxis results from the interchange of hyperpolarized and depolarized membrane potential; in steeply increasing gradients of egg peptide, continuous de novo activation of chemoattractant receptors maintains membrane hyperpolarization, suppressing Ca^{2+} entry and favoring straighter swimming trajectories. Upon entry into a negative SAP gradient, receptor activation falls, hyperpolarization transitions into depolarization and Ca^{2+} entry triggers a chemotactic turn. Elements of this proposed regulatory mechanism have been thrown into doubt by more recent single cell measurements which demonstrate that the straighter swimming episodes that intersperse the Ca^{2+} fluctuations often coincide with periods of elevated $[Ca^{2+}]_i$ (Bohmer et al., 2005; Shiba et al., 2008; Wood et al., 2005). Nevertheless, only minor conceptual adjustments are required to adapt this prior model to the results presented in this study. We propose that for *L. pictus* sperm undergoing chemotaxis, continuous activation of speract receptors in positive gradients leads to extended hyperpolarization of the membrane potential which accounts for the observed suppression of Type (+) Ca^{2+} fluctuations. Interestingly it has been shown that a cyclic nucleotide gated K^+ (CNGK) channel localized to the flagella of *A. punctulata* sperm shows slow inactivation kinetics (Bonigk et al., 2009), a property compatible with the generation of extended periods of hyperpolarized membrane potential. The hyperpolarization reverses once sperm enter a negative speract gradient, which after a typical ~200 ms delay leads to generation of a chemotactic turn that optimally reorients the sperm into swimming once more towards the source of the gradient. At some point during the subsequent straighter swimming phase in the positive speract gradient a hyperpolarized membrane potential is reestablished and extended by continuous speract receptor recruitment, which once again reverts to depolarized membrane potentials as sperm leave the positive gradient. This sets up a sequence of chemotactic turns, triggered by cycles of hyperpolarized/depolarized membrane potential that serve as the primary translators of the state of the extracellular chemoattractant gradient.

SAP receptor densities: a role in chemotactic motility regulation?

Sea urchin spermatozoa evolved high receptor densities, presumably to maximize the probability of binding once a chemoattractant molecule encounters the flagellum. It has been shown that *A. punctulata* spermatozoa are exquisitely sensitive, responding to femtomolar concentrations of resact (Kaupp et al., 2007; Kaupp et al., 2003). A density of ~14,000 resact receptors per *A. punctulata* spermatozoon has been calculated but it has been suggested that this could be underestimation of their true abundance (Kaupp et al., 2007). Previous calculations indicate that *L. pictus* spermatozoa have a three-fold greater number of receptors for speract than *S. purpuratus* spermatozoa ($6.3 \pm 0.5 \times 10^4$/cell vs. $2.0 \pm 0.9 \times 10^4$/cell), although the k_{on} and k_{off} values are similar in the two species (Nishigaki and Darszon, 2000; Nishigaki et al., 2001). The density of receptors may regulate the sensitivity to changes in binding rate and influence the delay times to increase flagellar Ca^{2+}. Possibly the lack of such significant bias in *S. purpuratus* spermatozoa is due to their lower speract receptor density which could explain their reduced sensitivity to this ligand (10^{-12}–10^{-6} M (Babcock et al., 1992)). Further studies are required to explore if the number of receptor sites are related to differences in navigation strategies employed by *L. pictus* and *S. purpuratus* spermatozoa.

Physiological context

Many marine animals produce vast numbers of gametes to contend with the enormous dilution that occurs with external fertilization in the sea. Other factors that increase fertilization probabilities include the temporal and spatial coordination of male and female gamete spawning, a relatively large oocyte (Podolsky, 2001), and the release of chemoattractants by the oocyte and/or its accessory structures (Miller, 1985a). There is evidence that the

limiting distance over which chemotaxis functions in marine species is within approximately 1 mm radial distance from the oocytes (Miller, 1985a; Ward et al., 1985; Yoshida et al., 1993). Within our experimental system the chemotactic response of *L. pictus* spermatozoa was confined to the limits of ~40–200 μm from the source of the speract gradient (Figs. 2, 4, S1 and S3), however this finding is somewhat artificial given the spatial limitations imposed on the speract gradient by the optical pathway employed to deliver the UV light pulse.

Although we could not directly determine the shape or magnitude of the speract gradient created within our experimental assay we can infer the speract concentration ranges that *L. pictus* spermatozoa were exposed based on phenomenological responses. Experimental and simulation data suggest that a chemoattractant concentration range of $10^{-9} \pm 10^{2}$ M is optimal for chemotaxis. Outside of this range, lower concentrations of chemoattractant are sub-optimal, whereas higher concentrations probably trigger adaptation mechanisms within intracellular signal transduction pathways that diminish chemoattractant-induced motility responses (Bohmer et al., 2005; Friedrich and Jülicher, 2008; Kaupp et al., 2003; Ward et al., 1985). At approximately 200 μm from the center of the UV illumination field we observed an outer limit for induced motility responses. This represents the absolute speract sensitivity limit for *L. pictus* spermatozoa that, from comparison to previous results, represents a speract concentration threshold below ~10^{-11}–10^{-12} M (Nishigaki and Darszon, 2000). *L. pictus* sperm inside this outer limit could be divided into two populations, proximal and central, according to their motility responses. It is possible that this proximal population, that undergoes chemotaxis, experiences speract concentrations in the range of 10^{-9}–10^{-11} M predicted to be optimal for chemotactic motility. Once these Proximal P. spermatozoa pass within an inner limit of ~40 μm from the source of the gradient they largely cease to generate Ca^{2+} fluctuations and chemotactic turns, reverting to low-curvature circular trajectories that often encircle the source of the speract gradient. The second population (Central P.) encompasses spermatozoa that are within the ~40 μm limit at the moment of speract gradient generation. These spermatozoa initially generate Ca^{2+} fluctuations and undergo turning events of increased frequency compared to the proximal population. Another key difference to the proximal population response is the distribution of the Ca^{2+} fluctuations relative to the direction of the speract gradient; unlike the proximal population that shows a clear bias towards Type (−) fluctuations, in the central population this bias is much less evident. Spermatozoa of the central population eventually switch to a motility pattern similar to that of newly arrived spermatozoa of the proximal population, namely low-curvature circular trajectories. It is possible that ~40 μm inner limit represents the transition to speract concentrations of 10^{-9}–10^{-8} M, a range predicted to be sub-optimal for chemotaxis due to adaptation of intracellular signaling mechanisms. Another possibility is that the relative steepness of the speract gradient is diminished in the center of the field, such that the central population indiscriminately initiate Type (−) and Type (+) Ca^{2+} fluctuations, whereas the steeper gradient present around the proximal population favors the bias towards the Type (−) Ca^{2+} fluctuations that drive chemotaxis in this population. We wish to note that the absolute concentration ranges mentioned are likely to vary for individual species and we mention them for comparative and illustrative, not definitive, purposes.

The accumulation of sperm at the source of the speract gradient is therefore dependent on two interacting parameters. The first is the relatively shallow chemoattractant gradient present, or concentrations of speract above the optimal range for chemotaxis, which promotes the generation of both Type (−) and Type (+) Ca^{2+} fluctuations with shorter straight swimming periods (an unfavorable combination for large lateral re-localization) that serves to trap the spermatozoa at the source of the gradient; the second is a temporal adaptation mechanism that imposes a limit on the generation of Ca^{2+} fluctuations, hence spermatozoa that do arrive at the source of the gradient soon lose the ability to generate the turning events that could promote their exit from the zone. The consequence is more locally confined motility patterns (seen in the central population, and the secondary phase of the response for the proximal population) that probably maximizes the likelihood of spermatozoa–egg union once spermatozoa arrive at source of the speract gradient (that is to say, in close vicinity of the oocyte). Whether this secondary motility phase is relevant in a physiological context is open to question. The ultimate source of the chemoattractant gradient is the egg, and once a sperm encounters its target it will become enveloped in the egg investments. Nevertheless, sea urchin sperm–egg encounters naturally occur in the open ocean, where chemoattractant gradients will readily become deformed and fragmented by the chaotic hydrodynamic forces operating. This will place environmentally-determined limits on the precision of sperm guidance mechanisms, for which the observed second-phase motility pattern may represent an adapted response.

The extensive limitations of the experimental model in reproducing the natural conditions encountered during sea urchin fertilization must also be taken into account when considering why chemotaxis has not been observed in *S. purpuratus* sperm. It is possible that limiting factors in the experimental design, such as the two dimensional constraint on sperm motility or the fixed speract gradient form, mask an ability of *S. purpuratus* sperm to redirect their trajectory towards a chemoattractant source. Even so, it is worth speculating why *S. purpuratus* spermatozoa might not have evolved a chemotactic mechanism for egg localization as part of their reproductive strategy. As already mentioned, sea urchin gametes normally encounter one another in a turbulent ocean, and the reproductive strategies of individual species are evolutionarily honed by the hydrodynamic properties of their environment (Riffell et al., 2004). In a natural habitat, chemical gradients are shaped by eddies, convection, and drifting of eggs rather than by homogeneous diffusion of chemoattractants. It has been shown that the laminar shear acting on the oocyte is of primary importance in determining whether chemotaxis is a viable strategy to enhance reproductive success in marine animals. As laminar shear values increase, chemoattractant plumes contract and fragment, to the eventual extent that information on the location of the oocyte is effectively lost (Riffell and Zimmer, 2007). In the case of the red abalone (*Haliotis rufescens*), whose spermatozoa undergo chemotaxis, the fertilization efficiency peaked sharply at levels of laminar shear similar to those found in its natural environment (Riffell and Zimmer, 2007). This suggests a natural physical limit on the degree of laminar shear compatible with long-range gamete communication, and we would not expect to encounter chemotaxis in spermatozoa of organisms that live in environments that habitually experience laminar shear levels above this permissive limit. The fertilization success of *S. purpuratus* gametes also varies according the degree of laminar shear experienced (Mead and Denny, 1995). We are currently examining such factors as a means to understand the presence or absence of chemotaxis as a strategy for enhancing reproductive success for individual species of sea urchin.

Our results advance our understanding of the mechanisms of chemotaxis in sea urchin spermatozoa, a model organism for studying signaling and regulation of the eukaryotic flagellum. Although arguably best characterized in marine organisms, spermatozoa chemotaxis has been observed in diverse taxa from bracken spermatozoa to various invertebrate and vertebrate organisms. Given the great degree of structural conservation of the flagella throughout evolution, these observations may be of relevance to spermatozoa guidance mechanisms, and control of flagellar and ciliary beating, in general.

Acknowledgments

The authors thank Dr. S. Baba for providing BohBoh software v3.29 and Adriana Santa-Maria for advice in α calculations. We also wish to thank Prof. Michael Whitaker for support and important suggestions throughout this project. This work was supported by grants from CONACyT (56660 to TN and 49113 to AD), NIH R01 HD038082-07A1 (to AD), PAPIIT (IN211907 to TN and IN211809 to AD) and the Wellcome Trust.

Appendix A. Supplementary data

Supplementary data associated with this article can be found, in the online version, at doi:10.1016/j.ydbio.2010.04.013.

References

Baba, S.A., Mogami, Y., 1985. An apporact to digital image analisys of bending shapes of eukaryotic flagella and cilia. Cell Motil. 5, 475–489.
Babcock, D.F., Bosma, M.M., Battaglia, D.E., Darszon, A., 1992. Early persistent activation of sperm K+ channels by the egg peptide speract. Proc. Natl. Acad. Sci. U. S. A. 89, 6001–6005.
Bentley, J.K., Garbers, D.L., 1986. Receptor-mediated responses of plasma membranes isolated from *Lytechinus pictus* spermatozoa. Biol. Reprod. 35, 1249–1259.
Bentley, J.K., Tubb, D.J., Garbers, D.L., 1986. Receptor-mediated activation of spermatozoan guanylate cyclase. J. Biol. Chem. 261, 14859–14862.
Bohmer, M., Van, Q., Weyand, I., Hagen, V., Beyermann, M., Matsumoto, M., Hoshi, M., Hildebrand, E., Kaupp, U.B., 2005. Ca2+ spikes in the flagellum control chemotactic behavior of sperm. EMBO J. 24, 2741–2752.
Bonigk, W., Loogen, A., Seifert, R., Kashikar, N., Klemm, C., Krause, E., Hagen, V., Kremmer, E., Strunker, T., Kaupp, U.B., 2009. An atypical CNG channel activated by a single cGMP molecule controls sperm chemotaxis. Sci. Signal. 2 ra68.
Brokaw, C.J., 1974. Calcium and flagellar response during the chemotaxis of bracken spermatozoids. J. Cell. Physiol. 83, 151–158.
Cook, S.P., Brokaw, C.J., Muller, C.H., Babcock, D.F., 1994. Sperm chemotaxis: egg peptides control cytosolic calcium to regulate flagellar responses. Dev. Biol. 165, 10–19.
Darszon, A., Beltran, C., Felix, R., Nishigaki, T., Trevino, C.L., 2001. Ion transport in sperm signaling. Dev. Biol. 240, 1–14.
Darszon, A., Nishigaki, T., Wood, C., Trevino, C.L., Felix, R., Beltran, C., 2005. Calcium channels and Ca2+ fluctuations in sperm physiology. Int. Rev. Cytol. 243, 79–172.
Darszon, A., Guerrero, A., Galindo, B.E., Nishigaki, T., Wood, C.D., 2008. Sperm-activating peptides in the regulation of ion fluxes, signal transduction and motility. Int. J. Dev. Biol. 52, 595–606.
Eisenbach, M., Giojalas, L.C., 2006. Sperm guidance in mammals — an unpaved road to the egg. Nat. Rev. Mol. Cell Biol. 7, 276–285.
Friedrich, B.M., Jülicher, F., 2008. The stochastic dance of circling sperm cells: sperm chemotaxis in the plane. New J. Phys. 10, 1367–2630.
Galindo, B.E., Beltran, C., Cragoe Jr., E.J., Darszon, A., 2000. Participation of a K(+) channel modulated directly by cGMP in the speract-induced signaling cascade of *Strongylocentrotus purpuratus* sea urchin sperm. Dev. Biol. 221, 285–294.
Galindo, B.E., de la Vega-Beltran, J.L., Labarca, P., Vacquier, V.D., Darszon, A., 2007. SptetraKCNG: a novel cyclic nucleotide gated K(+) channel. Biochem. Biophys. Res. Commun. 354, 668–675.
Granados-Gonzalez, G., Mendoza-Lujambio, I., Rodriguez, E., Galindo, B.E., Beltran, C., Darszon, A., 2005. Identification of voltage-dependent Ca2+ channels in sea urchin sperm. FEBS Lett. 579, 6667–6672.
Hansbrough, J.R., Garbers, D.L., 1981. Speract. Purification and characterization of a peptide associated with eggs that activates spermatozoa. J. Biol. Chem. 256, 1447–1452.
Kaupp, U.B., Solzin, J., Hildebrand, E., Brown, J.E., Helbig, A., Hagen, V., Beyermann, M., Pampaloni, F., Weyand, I., 2003. The signal flow and motor response controling chemotaxis of sea urchin sperm. Nat. Cell Biol. 5, 109–117.
Kaupp, U.B., Kashikar, N.D., Weyand, I., 2007. Mechanisms of sperm chemotaxis. Annu. Rev. Physiol.
Mead, K.S., Denny, M.W., 1995. The effects of hydrodynamic shear stress on fertilization and early development of the purple sea urchin *Strongylocentrotus purpuratus*. Biol. Bull. 188, 46–56.
Miller, R., 1985a. Sperm chemo-orientation in the metazoa. In: Metz, C., Monroy, A. (Eds.), Biology of Fertilization. Academic Press, New York, pp. 275–337.
Miller, R., 1985b. Sperm chemo-orientation in the metazoa. : Biology of Fertilization, vol. 1. Academic, New York, pp. 275–337.
Nishigaki, T., Darszon, A., 2000. Real-time measurements of the interactions between fluorescent speract and its sperm receptor. Dev. Biol. 223, 17–26.
Nishigaki, T., Zamudio, F.Z., Possani, L.D., Darszon, A., 2001. Time-resolved sperm responses to an egg peptide measured by stopped-flow fluorometry. Biochem. Biophys. Res. Commun. 284, 531–535.
Nishigaki, T., Wood, C.D., Tatsu, Y., Yumoto, N., Furuta, T., Elias, D., Shiba, K., Baba, S. A., Darszon, A., 2004. A sea urchin egg jelly peptide induces a cGMP-mediated decrease in sperm intracellular Ca(2+) before its increase. Dev. Biol. 272, 376–388.
Podolsky, R.D., 2001. Evolution of egg target size: an analysis of selection on correlated characters. Evol. Int. J. Org. Evol. 55, 2470–2478.
Podolsky, R.D., 2002. Fertilization ecology of egg coats: physical versus chemical contributions to fertilization success of free-spawned eggs. J. Exp. Biol. 205, 1657–1668.
Riffell, J.A., Zimmer, R.K., 2007. Sex and flow: the consequences of fluid shear for sperm egg interactions. J. Exp. Biol. 210, 3644–3660.
Riffell, J.A., Krug, P.J., Zimmer, R.K., 2004. The ecological and evolutionary consequences of sperm chemoattraction. Proc. Natl. Acad. Sci. U. S. A. 101, 4501–4506.
Shiba, K., Baba, S.A., Inoue, T., Yoshida, M., 2008. Ca2+ bursts occur around a local minimal concentration of attractant and trigger sperm chemotactic response. Proc. Natl. Acad. Sci. U. S. A. 105, 19312–19317.
Strunker, T., Weyand, I., Bonigk, W., Van, Q., Loogen, A., Brown, J.E., Kashikar, N., Hagen, V., Krause, E., Kaupp, U.B., 2006. A K(+)-selective cGMP-gated ion channel controls chemosensation of sperm. Nat. Cell Biol. 8, 1149–1154.
Suzuki, N., 1995. Structure, function and biosynthesis of sperm-activating peptides and fucose sulfate glycoconjugate in the extracellular coat of sea urchin eggs. Zoolog. Sci. 12, 13–27.
Suzuki, N., Nomura, K., Ohtake, H., Isaka, S., 1981. Purification and the primary structure of sperm-activity peptides from the jelly coat of sea urchin eggs. Biochem. Biophys. Res. Commun. 99, 1238–1244.
Tatsu, Y., Nishigaki, T., Darszon, A., Yumoto, N., 2002. A caged sperm-activating peptide that has a photocleavable protecting group on the backbone amide. FEBS Lett. 525, 20–24.
Ward, G.E., Brokaw, C.J., Garbers, D.L., Vacquier, V.D., 1985. Chemotaxis of *Arbacia punctulata* spermatozoa to resact, a peptide from the egg jelly layer. J. Cell Biol. 101, 2324–2329.
Wood, C.D., Darszon, A., Whitaker, M., 2003. Speract induces calcium oscillations in the sperm tail. J. Cell Biol. 161, 89–101.
Wood, C.D., Nishigaki, T., Furuta, T., Baba, S.A., Darszon, A., 2005. Real-time analysis of the role of Ca(2+) in flagellar movement and motility in single sea urchin sperm. J. Cell Biol. 169, 725–731.
Wood, C.D., Nishigaki, T., Tatsu, Y., Yumoto, N., Baba, S.A., Whitaker, M., Darszon, A., 2007. Altering the speract-induced ion permeability changes that generate flagellar Ca2+ spikes regulates their kinetics and sea urchin sperm motility. Dev. Biol. 306, 525–537.
Yoshida, M., Inaba, K., Morisawa, M., 1993. Sperm chemotaxis during the process of fertilization in the ascidians *Ciona savignyi* and *Ciona intestinalis*. Dev. Biol. 157, 497–506.
Yoshida, M., Murata, M., Inaba, K., Morisawa, M., 2002. A chemoattractant for ascidian spermatozoa is a sulfated steroid. Proc. Natl. Acad. Sci. U. S. A. 99, 14831–14836.